Intrinsic Anion Vacancies in Monolayer Transition Metal Dichalcogenides

Y. Guo[1], D Liu[2], and J. Robertson[1]

[2]Department of Engineering, Cambridge University, Cambridge CB2 1PZ, United Kingdom

[1]State Key Laboratory of Tribology, Tsinghua University, Beijing, 100084, China

Abstract: It is predicted that the Schottky barriers of the transition metal dichalcogenides WS_2, $MoSe_2$, WSe_2, $MoTe_2$, and WTe_2 will suffer from less Fermi level pinning than MoS2 due to anion vacancies, because their vacancy formation energies is larger. The anion vacancy levels of WS2, WSe2, and MoSe2 and MoTe2 are also calculated to lie nearer midgap, so that ambipolar conduction should be easier in these compounds than in MoS2.

There has been particular interest in using transition metal dichalcogenide (TMD) layer compounds, MX_2 where M=Mo/W, X=S/Se/Te) for electronic and photonic devices, in particular for their use as field effect transistors (FETs) and tunnel FETs (tFETs). Nevertheless there is a problem with using the most common TMD, MoS_2, because of its high device contact resistance, and the difficulty of it achieving bipolar operation. The problem arises from the presence of Schottky barriers at its contacts. Generally, the Schottky barrier heights (SBHs) ϕ_n of different metals on a semiconductor will vary with the metal work function Φ_M according to a pinning factor $S = d\phi_n/d\Phi_M$, with S varying between the strongly pinned limit of S=0 and the weakly pinned limit of S=1. The less pinning of the SBH, the more it is possible to control the SBH by just varying the work function of the contact metal, so that it spans the semiconductor's band gap.

Generally, the pinning factor decreases as the density of gap states N at the metal-semiconductor interface increases, according to

$$S = \frac{1}{1 + \frac{N\delta e^2}{\varepsilon}}$$

where δ in the decay length of the states, e is the electronic charge and ε is the local dielectric constant. These gap states can be either the intrinsic metal induced gap states (MIGS) or states due to extrinsic defects. It has been expected by some that the presence of van der Waals bonding between the TMD layers would extend to their contacts, so this would reduce N and thereby increase S, so that the SBH would be readily controllable. In fact, even the top contacts between most metals tend to form quite short bonds to the outer chalcogen atoms, and thus the supposed van der Waals bonding does not occur at the contacts. This leads to calculated Schottky barrier pinning factors of $S \sim 0.3$ for both the bulk and monolayer TMDs [x].

More interestingly, experimentally, Das et al [4] found that there was stronger pinning than this, with a pinning factor of $S \sim 0.10$. This implies that the interfaces possess additional gap states due to defects than increase the pinning (decrease the pinning factor) beyond the MIGS limit. Previously, Liu et al [x] noted the presence of S vacancy defects in transmission electron

microscopy images. Liu et al [8] showed that such S vacancies would cause the SBH pinning in the gap at the observed energy range. Then Gong et al [21] noted a strong influence of deposition conditions on the behavior of metal contacts on MoS2 which they attributed to the formation of defects.

Thus it is worthwhile to consider the pinning behavior on other TMDs, if we can find TMDs which have large vacancy formation energies to inhibit vacancy formation, or TMDs with pinning energies nearer mid gap. This would at least return S to a value nearer to defect –free limit, and allows some degree of control on the SBHs. It would also allow more ambi-polar behavior. Here, we carry out defect calculations that show that a number of selenide and telluride TMDs satisfy this condition.

Our electronic structure calculations use density functional theory (DFT) to describe the electron-electron interactions. However, DFT is known to under-estimate band gaps of semiconductors and insulators. Thus, we supplement the DFT calculations with calculations using the screened exchange (sX) hybrid density functional for both the band structures and the defect states.

The calculations are carried out in the CASTEP plane-wave pseudopotential code [45]. Norm-conserving pseudopotentials are needed for the sX calculations. Spin-orbit coupling is not included. A cutoff energy of 680eV converges the total energy to less than 0.01eV per atom. The atomic structure is fully relaxed with a residual force of less than 0.02eV/Å^{-1}. The Brillouin zone integrations use a 2×2×2 Monkhorst-Pack grid in total energy calculation and geometry relaxation and a 3×3×3 grid for calculating the density of states (DOS). A rectangular 6x6 supercell is used for the defect calculations. This supercell geometry maximizes the spacing between defect images with a minimum spacing is 15.0 Å between defect images. A vacuum layer of 20 Å is inserted between the layers, which gives a good convergence of band gap.

The charge transition states of intrinsic defects are calculated using the supercell method. Corrections for defect charges and band occupations as in ref 47. The total energy of the perfect supercell (E_H) and the supercell with defect (E_q) has been calculated with different charge states. The defect formation energy H_q is then given by

$$H_q(E_F,\mu) = [E_q - E_H] + q(E_V + \Delta E_F) + \sum_\alpha n_\alpha(\mu_\alpha^0 + \Delta\mu_\alpha)$$

Here, qE_v is the change of Fermi energy when charge q is added, n_α is the number of atoms of species α, and μ_α is the relative chemical potential of element α. There is no extra correction needed for two-dimensional calculation. The chalcogen chemical potential in the chalcogen-rich limit is that of crystalline phase, taken as 0 eV. The S_8 molecule is used for S while the trigonal crystal phase is used for Se and Te. Correspondingly, the chalcogen-poor limit is the metal-MX_2 equilibrium, which equals the heat of formation of MX_2 divided by two the number of chalcogen atoms per formula unit. The experimental heats of formation are summarized in Table 1.

The band structures of monolayer MX_2 in the 2H polytype calculated in the sX method are shown in Figs 1. The lattice constants and band gaps are summarized in Tables 1 and 2, compared with experimental band gaps. The valence band maximum (VBM) is set to be 0 eV in all figures. The electronic structures for other TMDs are similar to MoS_2. Bulk MX_2 has a calculated indirect smaller band gap than the direct band gap of the corresponding monolayer MX_2. In bulk MX_2, the VBM is at Γ while the conduction band minimum (CBM) is at K. The band structures of all six MX_2 compounds are overall quite similar. The Mo compounds have a larger band gap than the W compounds, in both the bulk and the monolayers. This is because a

large part of the band gap arises from the crystal field splitting of the metal d states, and this is large for the heavier metal, W.

Our band structures are consistent with experiment and they have a similar dispersion to the GW results. The partial DOS of Mo and S also confirms that both VBM and CBM away from K are both hybridized Mo 4d and S 3p orbitals. It is noted that the band gap from sX is close to the optical gap rather than the fundamental gap, which has been observed in previous hybrid density functional studies.

We consider vacancy defects in TMDs. For metal vacancies, we must break six M-X bonds, whereas for chalcogen vacancies, we must only break three M-X bonds. This makes the vacancy formation energy much smaller for the chalcogen vacancy, and indeed the chalcogen vacancy is found to dominate transmission electron microscope images of MoS2 surfaces [x]. The Mo vacancy formation energy in MoS_2 was calculated to be 8.02eV, three times larger than S vacancy formation energy [x]. Here, a similar trend is found for the other TMD compounds. Thus, we discuss only the chalcogen vacancy from now on.

The calculated formation energies of the neutral chalcogen vacancy V^0 is given in Table 2, all in the sX functional. The S vacancy in MoS_2 has been studied previously. The 0/-1 and -1/-2 transition states are calculated to lie in the upper gap. The formation energy of V^0 in the S-rich condition is 2.35eV. We then move to the other materials in the MX_2 family. In MoSe2, the formation energy in Se rich condition is 2.82 eV for V^0, significantly larger than for the S vacancy in MoS_2. The defect levels in the band gap are both lower in $MoSe_2$ than in MoS_2, as shown in Table 2 and Fig.2(a,b).

This could be explained by the band offset of MoS_2 and $MoSe_2$. The CBM is determined by the hybridization of Mo d orbital and chalcogen p orbital. The Se p orbital lies higher than the S orbital, so the CBM for $MoSe_2$ is higher than inMoS_2. The defect level is composed of Mo d orbitals, which should stay almost the same depth for MoS_2 and $MoSe_2$. Therefore the defect level of Se vacancy becomes relatively deeper in the band gap compared with MoS_2.

The results for WS_2 are shown in Fig.2(d). The formation energy for V^0 in the S-rich condition is 3.38eV, larger than that of MoS_2. In the S-poor case the formation energy is shifted down by 1.26eV. However in both limits the formation energy is always positive. When the Fermi level is close to CBM, the formation energy is still about 1.0eV. The larger vacancy formation energy indicates that it is the vacancy concentration in WS_2 is much smaller than that of MoS_2. The defect transition levels are similar, 0/-1 and -1/-2 at 1.25 eV and 1.27eV. The defect levels are much deeper considering the large band of 2.02eV. Considering both the formation energy and defect level in the band gap, we predict that the Fermi level pinning effect observed in MoS_2 should be not obvious in WS_2.

Fig.2(c) shows the transition level and formation energy for $MoSe_2$. The similar trend has been observed just like the previous materials. The formation energy for Se vacancy of WSe_2 is smaller than that of $MoSe_2$ due to the weaker bonding of M-Se. The CBM is further shifted up compared with WS_2 but the W dangling bonds should stay almost the same. Therefore the defect level is pushed down. The two transition levels are at 0.72eV and 0.94eV respectively. The formation energy also keeps positive in both Se-rich and Se-poor limit no matter where Fermi level is.

The transition level for $MoTe_2$ and WTe_2 is shown in Figure 2 (d) and (e). Te has the same valence as Se and S. The Te bond is even weaker than the S and Se bond. The lattice constant of telluride is significantly larger and the enthalpy of heat is smaller than the corresponding sulfide and selenide. The formation energy of vacancy for $MoTe_2$ and WTe_2 is almost the same in

neutral state, 3.05eV and 3.06eV. The formation energy is still much larger than that of S vacancy in MoS_2. When the Fermi level is close to CBM, the formation energy is about 1.30eV and 0.94eV even in Te-poor condition. This means that it is almost impossible to create the Te vacancy by tuning the chemical potential of Te during growth. The larger defect structure is still the same as in other MX_2. The two transition states are deep in the mid-gap region. However, due to the smaller band gap of telluride, the gaps are not as deep as in sulphide and selenide. It is worth noting that we used 2H phase for telluride, the same as other MX_2. Recently it is reported that $MoTe_2$ is also stable in a distorted semi-metallic phase [53]. For transistor application we only consider the 2H semiconducting phase in this work.

We have compared the anion vacancy defect levels in MX_2 monolayer in Fig.3. The band edges are aligned according to the charge neutrality levels listed in Table 1. The chemical trend is quite obvious. The VBM is shifted up and CBM shifted down when anion goes up. The defect levels are the metal d orbitals determines the absolute position of the S vacancy while the CBM changes the relatively position of the defect states in the band gap. MoS_2 has the lowest band edges, leading to the most shallow S vacancy state to the CBM. The formation energy of X vacancy becomes larger when Se/Te substituting S or W substituting Mo. The shift-up of band edges decreases the work function of the material. This could also facilitate the p-type doping and conductance induced by the large work function metal electrode such as Pt and MoO_3-x. In our previous work the n-type dominated conductance in MoS_2-based devices could be explained by S vacancy [36]. The large vacancy formation energy and deep transition level suggest that it is easier to get p-type conductance in MX_2 monolayer other than MoS_2. Recently ambipolar WSe_2 device has been fabricated with Pt contact [22].

In conclusion, the S and Se vacancy defect of monolayer MX_2 has been calculated by the sX hybrid functional. The S/Se vacancy has much lower formation energy than the Mo/W vacancy. The S/Se vacancies are all found to introduce 0/+1 and +1/+2 transition states in the band gap. The transition levels are deep in the mid-gap region in $MoSe_2$, WS_2, and WSe_2. The formation energy of anion vacancies is much larger than that in MoS_2. The formation energy is always positive if Fermi level is close to the conduction band in the chalcogen-poor limit. The Fermi level pinning near the conduction band edge due to reactive metal electrode should be suppressed in MX_2 other than MoS_2.

The authors are grateful for financial support from the National Natural Science Foundation of China (Grant No.51105222), Beijing Research Program (Grant No. 100322002).

1 K. F. Mak, C. Lee, J. Hone, J. Shan, and T. F. Heinz, Phys Rev Lett **105** 136805 (2010).
2 B Radisavljevic, A Radenovic, J Brivio, V Giacometti, A Kis, Nature Nano **6** 147 (2011)
3 D Jariwala, VK Sangwan, L J Lauhon, T J Marks, M C Hersam, ACS Nano 8 1102 (2014)
4 S. Das, H. Y. Chen, A. V. Penumatcha, and J. Appenzeller, NanoLett **13**, 100 (2013)
5 H Wang, L Yu, Y H Lee, Y Shi, A Hsu, M L Chin, L J Li, M Dubey, J Kong, T Palacois, NanoLett **12** 4674 (2012)
6 Y J. Zhang, J. T. Ye, Y. Matsuhashi, and Y. Iwasa, Nano Lett **12**, 1136 (2012).
7 H Liu, A T Neal, P D Ye, ACS Nano **6** 8563 (2012)
8 W. Liu, J. H. Kang, D. Sarkar, Y. Khatami, D. Jena, and K. Banerjee, Nano Lett **13**, 1983 (2013).
9 N R Pradhan, D Rhodes, Q Zhang, S Talapatra, M Terrones, P M Ajayan, L Balicase, App Phys Lett **102** 123105 (2013)
10 W Bao, X Cai, D Kim, K Sidhara, M S Fuhrer, App Phys Lett **102** 042104 (2013)
11 S Das, A Prakash, R Salazar, J Appenzeller, ACS Nano **8** 1681 (2014)
12 S Das, J Appenzeller, App Phys Lett 103 103501 (2013)
13 C Gong, H Zhang, W Wang, L Colombo, R M. Wallace, K J Cho, App Phys Lett 103 053513 (2013)
14 Qiu, H.; Pan, L. J.; Yao, Z. N.; Li, J. J.; Shi, Y.; Wang, X. R. Appl. Phys. Lett. 100, 123104. (2012)
15 S Chuang, C Battaglia, A Azcatl, S McDonnell, J S Kang, X Yin, M Tosun, R Kapadia, H Fang, R M. Wallace, and A Javey, Nano Lett 14, 1337 (2014)
16 W. Zhang, M. Chiu, C.-H. Chen, W. Chen, L.-J. Li, A. T. S. Wee, ACS Nano, 8, 8653(2014)
17 S McDonnell, R Addou, C Buie, R M. Wallace, C L. Hinkle, ACS Nano, 8, 2880 (2014).
18 W. Zhou, X Zou, S Najmaei, Z Liu, Y Shi, J Kong, J Lou, P M Ajayan, B I Yakobson, J C Idrobo, Nano Lett 13, 2615 (2013).
19 C. Gong, S. McDonnell, X. Qin, A. Azcati, H. Dong, Y.J. Chabal, K.J. Cho, R. M. Wallace, ACS Nano 8, 642 (2014).
20 Popov, I.; Seifert, G.; Tomanek, D. Phys. Rev. Lett. 108, 156802 (2012).
21 C Gong, L Colombo, R M. Wallace, K J Cho, Nano Lett., 14, 1714 (2014)
22 D. Liu, Y. Guo, L. Fang, J. Robertson App Phys Lett 102 042104 (2013)
23 Cowley and Sze, JAP (1979)
24 W Monch, PRL (1986)
25 Y. Guo, D. Liu, J Robertson, in Review (2015)
26 S. J. Clark and J. Robertson, Phys Rev B 82 085208 (2010).
27 D. Liu, S. J. Clark, and J. Robertson, Appl Phys Lett 96 032905 (2010).
28 S. J. Clark, M. D. Segall, C. J. Pickard, P. J. Hasnip, M. J. Probert, K. Refson, and M. C. Payne, Kristallogr. 220, 567 (2005).
29 S. Lany and A. Zunger, Phys Rev B 78 235104 (2008).
30 P A G O'Hare, B M Lewis, B A Parkinson, J Chem Thermodynamics **20** 681 (1988)
31 P A G O'Hare, I R Tasker, J M Tarascon , J Chem Thermodynamics 19 61 (1988)
32 P.A.G. O'Hare, W.N. Hubbard, G.K. Johnson, H.E. Flotow, J Chem Thermodynamics 16 45 (1984)
33 M. N. Ali, J. Xiong, S. Flynn, J. Tao, Q. D. Gibson, L.M. Schoop, T. Liang, N. Haldolaarachchige, M. Hirschberger, N. P. Ong, R.J. Cava, Nature 514, 205(2014)

Table 1 The used enthalpy of heat and calculated formation energy for MX_2.

	MoS_2	$MoSe_2$	$MoTe_2$	WS_2	WSe_2	WTe_2
Enthalpy of Heat	2.81 [48]	2.43 [49]	1.88 [51]	2.50 [50]	1.92 [48]	0.79 [52]
Vacancy formation energy	2.35	2.82	3.06	3.38	2.81	3.05

Table 1 The lattice constants, charge neutrality levels, and band gaps from sX and experiments in all monolayer MX_2

	Lattice Constant , Å	sX Band Gap, eV	CNL ,eV SX	Optical gap (Experiment) ,eV
MoS_2	3.17	1.88	0.95	1.84
$MoSe_2$	3.29	1.71	0.84	1.66
$MoTe_2$	2.36	1.46	0.72	
WS_2	3.16	2.13	1.07	1.94-2.05
WSe_2	3.36	1.82	0.73	
WTe_2	3.51	1.31	0.6	

Fig. 1. The band structure for the monolayer MX_2 . (a)WSe_2, (b) WS_2, (c)$MoSe_2$.

Fig. 2. Charge transition states for the Se/S/Te vacancies in sX.(a)MoSe2, (b)WS_2, (c)WSe_2 (d)$MoTe_2$ (e) WTe_2

Fig. 3. Comparisons of the defect levels in MX_2 monolayer aligned with respect to CNL.

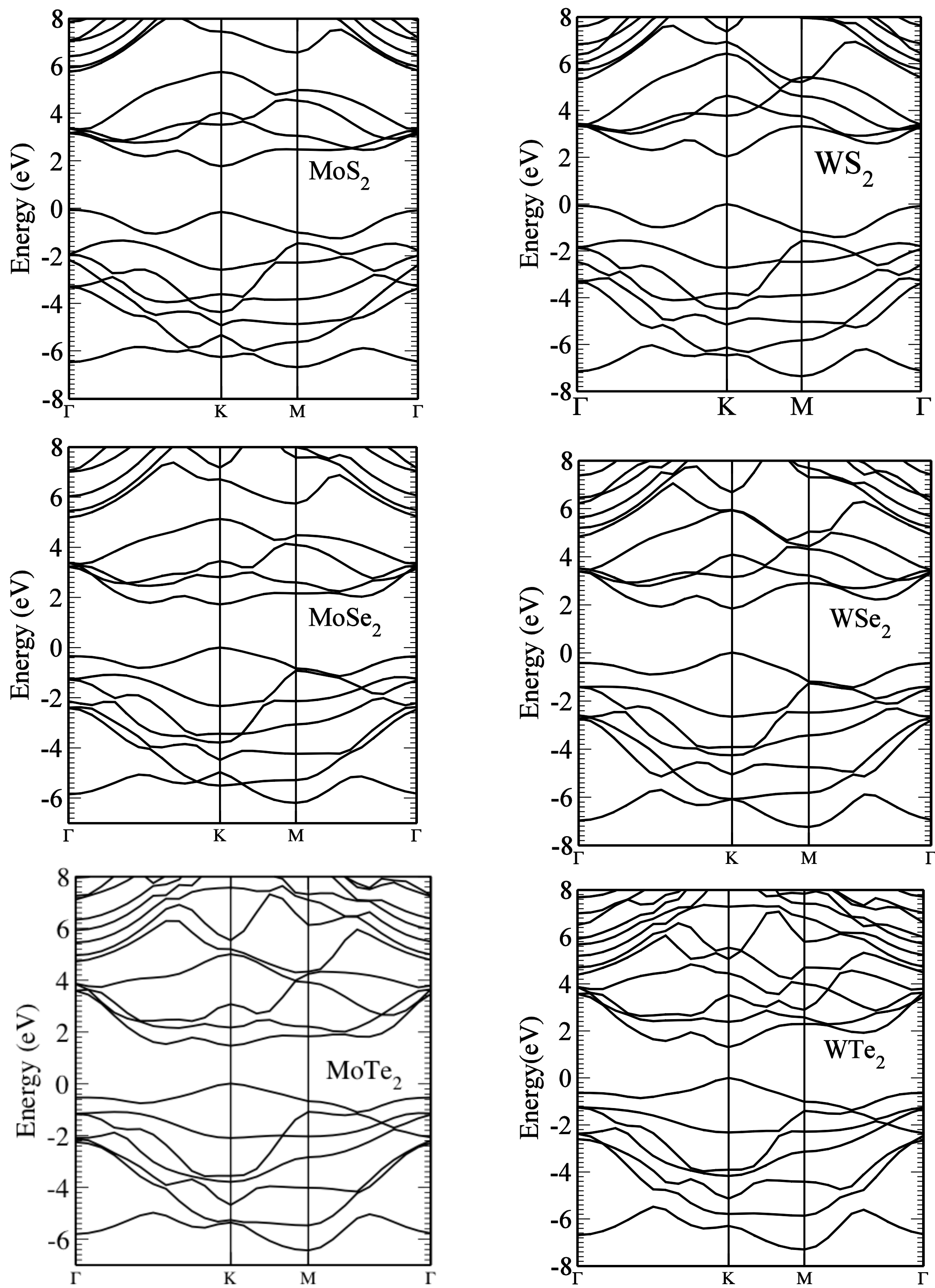

Fig. 1

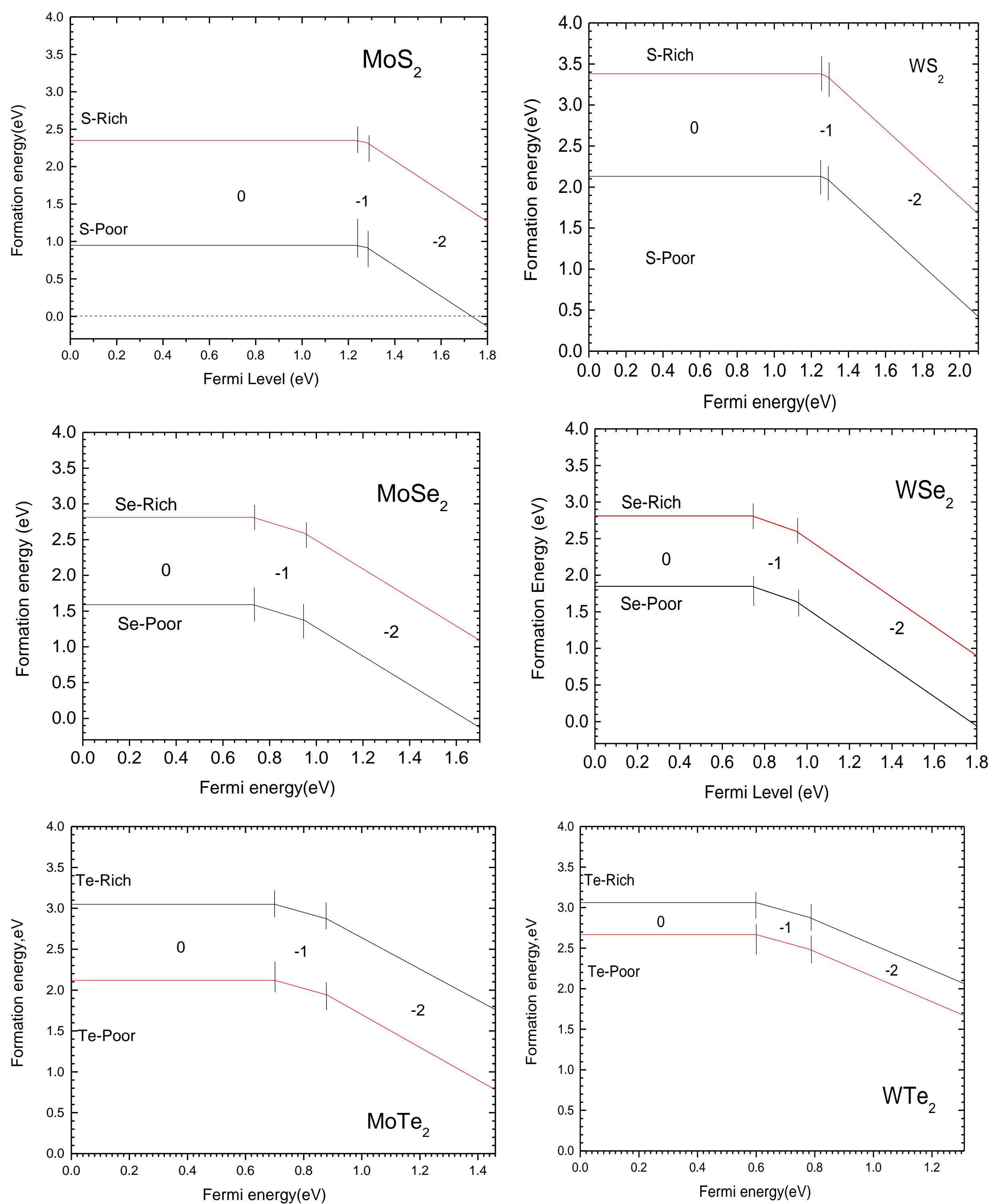

Fig. 2

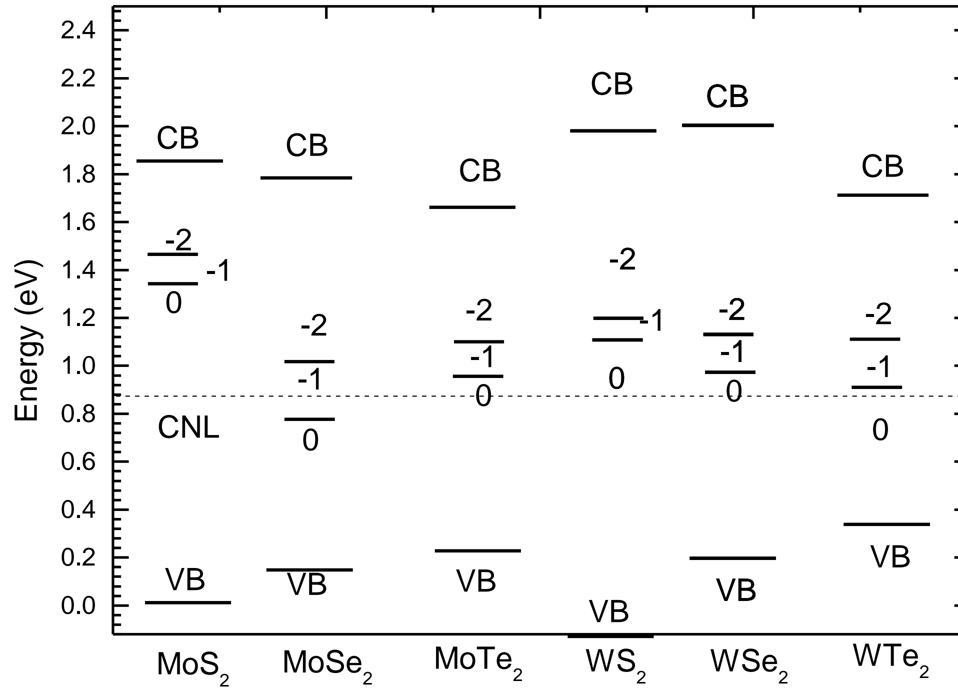

Fig. 3